

## Abrupt drainage of Lago Greve, a large proglacial lake in Chilean Patagonia, observed by satellite in 2020

Shuntaro Hata <sup>1,2</sup>, Shin Sugiyama <sup>1</sup> & Kosuke Heki <sup>3,4</sup>

Glacial lakes are increasing in number and extent under a warming climate. Despite demand for lake monitoring and understanding outburst mechanisms, studies of large outburst events are sparse. Here we report an outburst of Lago Greve, a large proglacial lake in Chilean Patagonia. During the event in April–July 2020, the lake level dropped by  $18.3 \pm 1.2$  m and the area decreased by  $14.5 \pm 0.02$  km<sup>2</sup>. The total water discharge was  $3.7 \pm 0.2$  km<sup>3</sup>, which is one of the largest glacial lake outbursts ever reported in satellite era. Satellite data indicated the collapse of a bump near the lake outlet triggered the event, by initiating erosion of the bank and bed of the outlet stream. Satellite gravimetry captured a signal of the event, although the magnitude of the corresponding mass change was inconsistent with the drained water mass. Our study demonstrated the potential for observing lake outburst using satellite imagery, altimetry, photogrammetry, and gravimetry.

<sup>1</sup>Institute of Low Temperature Science, Hokkaido University, Sapporo, Japan. <sup>2</sup>Graduate School of Environmental Science, Hokkaido University, Sapporo, Japan. <sup>3</sup>Department of Earth and Planetary Sciences, Hokkaido University, Sapporo, Japan. <sup>4</sup>Shanghai Astronomical Observatory, Chinese Academy of Sciences, Shanghai, China. ✉email: [shuntaro.hata@frontier.hokudai.ac.jp](mailto:shuntaro.hata@frontier.hokudai.ac.jp)

As a consequence of glacier retreat under a warming climate, the number, area, and volume of glacial lakes has increased in recent decades<sup>1</sup>. In particular, rapid increase has been observed in Patagonia<sup>2</sup>, Alaska<sup>3</sup>, Himalaya<sup>4</sup>, and Greenland<sup>5</sup>. Glacial lakes affect ice dynamics, frontal ablation, and hence the evolution of glaciers terminating in the lakes<sup>6–9</sup>. Because of the lake influences, freshwater calving glaciers experience more rapid retreat and greater mass-loss than glaciers terminating on land<sup>10</sup>. In Patagonia, freshwater calving glaciers are rapidly retreating and thinning<sup>11–14</sup>, which causes rapid mass loss of the Southern and Northern Patagonia Icefields<sup>15</sup>. As a result of the glacier retreat, glacial lakes in the regions are expanding at the greatest rate in the world<sup>1</sup>. Freshwater calving is important also because glaciers affect lake environments via nutrient-rich meltwater discharge<sup>16,17</sup>, sedimentation and water circulation<sup>18,19</sup>, which play critical roles in the ecosystems of the lakes<sup>20</sup>. Further, glacial lake outburst flood (GLOF) has a strong impact on physical and biological environments downstream<sup>21</sup>. For example, large-scale GLOFs during the deglaciation of past ice sheets affected ocean current and hence regional climate by discharging a large amount of freshwater into the ocean<sup>22,23</sup>. Monitoring glacial lakes is thus important for understanding future changes of freshwater calving glaciers and the surrounding environment.

GLOF occurs when a moraine-, glacier-, or bedrock-dam is breached. Tsunami and seiche waves generated by e.g., calving, landslide, or rockfall trigger outburst by initiating lakewater overflow and subsequent erosion of the dam<sup>24,25</sup>. Seepage of lakewater through a moraine dam and uplift of an ice dam due to flotation are other mechanisms that trigger lake outburst<sup>26,27</sup>. GLOF also occurs when a moraine dam spontaneously collapses after deglaciation, a process so called “self-destruction” of a dam<sup>28</sup>. Sudden release of a large amount of water has the potential to cause serious damage to communities and infrastructure downstream<sup>29</sup>. Several thousand deaths due to GLOFs have been reported during the last hundred years<sup>30</sup>. The actual number of fatalities is most likely greater because the inventory of lake outburst is incomplete<sup>31</sup>. Under the influence of formation and expansion of glacial lakes<sup>1–5</sup>, the frequency of GLOFs possibly increases in the 21st century<sup>32</sup>. Therefore, further understanding of outburst mechanism and long-term monitoring of glacial lakes are required to manage hazards in mountainous regions.

Satellite remote sensing techniques are powerful tools to monitor glacial lakes. For example, satellite images have been used to map glacial lakes and measure aerial changes all over the world<sup>1</sup>. Satellite observations were utilized to quantify the changes in Himalayan glacial lakes from 1990 to 2015 with temporal resolution of 5 years<sup>33</sup>. Lake surface elevations have been measured by satellite laser/radar altimetry<sup>34,35</sup> as well as digital elevation models (DEMs)<sup>36</sup>. Data series of Gravity Recovery And Climate Experiment (GRACE) and GRACE-FO (follow-on) have been combined with laser and radar altimeter measurement to quantify the water mass change of ordinary lakes<sup>37,38</sup>. Yi et al.<sup>39</sup> demonstrated an ability of the GRACE data to identify the change of 13.0 Gt of water of a reservoir. Nevertheless, GRACE has never been applied to GLOFs.

In April 2020, we observed a sudden retreat of the shoreline of Lago Greve, an extraordinarily large proglacial lake in Patagonia (Fig. 1). Additional analyses with several types of satellite data indicated the release of a large amount of water within a short time period. In this paper, we report changes in the lake area, water level, and volume during the event, as well as its impact on the gravity field. We also investigate the mechanism of drainage based on satellite imagery and DEMs. The data illustrates the details of a largest glacial lake outburst event observed by satellite to date.

**Study site.** Lago Greve (49.0°S, 73.9°W) is a glacier-fed lake situated on the western side of the Southern Patagonia Icefield (SPI) (Fig. 1). In November 2020, the lake covered an area of 187.9 km<sup>2</sup>, making it the fourth largest proglacial lake in the world<sup>1</sup>. Although no lake-depth measurement is available, the depth was estimated to be ≤150 m near the ice-front of the northern terminus of Glaciar Pío XI based on the lakebed geometry observed before the formation of the lake<sup>40,41</sup>. The lakewater drains through a gorge at the northwestern margin of the lake, where an outlet stream falls off to a marginal lake of Glaciar Occidental over steep terrain with an elevation difference of ~130 m (Fig. 1). From the lake outlet, water flows through fjords for a distance of ~130 km before entering into the Pacific Ocean.

The lake is fed by a number of outlet glaciers of the SPI, including Glaciar Pío XI, the largest glacier in Patagonia (Fig. 1). Between 1945–1962, Glaciar Pío XI advanced and blocked Río Greve, a stream from an outwash plain feeding into Eyre Fjord (e.g., ref. 42). The blocking resulted in the formation of Lago Greve as an ice-dammed lake (e.g., ref. 42). After the formation of Lago Greve, between 1945–1962, rapid lake drainage has never been reported. In recent decades, the lake is fed by seven glaciers, the northern glacier front and one of the subsidiary outlet glaciers of Glaciar Pío XI, Glaciar Lautaro, and two outlet glaciers from each of Glaciar Greve and Glaciar HPS-8 (Fig. 1).

## Results and discussion

**Drainage event.** The lake gradually enlarged from 2016 to 8 April 2020, resulting in an areal increase of  $3.1 \pm 0.02$  km<sup>2</sup> (Fig. 2a). This change was mostly due to the retreat of glaciers terminating in the lake ( $2.5 \pm 0.1$  km<sup>2</sup>). Sudden retreat of the shoreline was observed from the images on 8 April and 5 May 2020, followed by further retreat and lake area reduction of  $14.5 \pm 0.02$  km<sup>2</sup> from 8 April to 29 July 2020. The water surface dropped by  $12.3 \pm 2.7$  m from 8 to 29 April and  $18.3 \pm 1.2$  m from 8 April to 29 July, whereas change before the event was insignificant ( $\pm 1.2$  m) (Fig. 2b). Based on the relocation of the outlet stream (Fig. 3a–d) as well as the displacement of the lake margin (Fig. 3e–h), the onset of the drainage was determined as between 9 and 19 April 2020. After the drainage event, from 29 July to 1st November 2020, the lake area and water level were stable within the uncertainty ranges (Fig. 2a, b). The lake area on 1st November 2020 was  $187.9 \pm 0.02$  km<sup>2</sup>, indicating a 7.2% reduction since 8 April 2020. Water volume released from 8 April to 29 July 2020 was  $3.7 \pm 0.2$  km<sup>3</sup> ( $3.7 \pm 0.2$  Gt), according to the lake area and the changes in water level. This is equivalent to  $31 \pm 8\%$  of annual ice mass loss from the SPI observed in 2000–2015/16 (ref. 43) and 0.01 mm of sea level rise.

The magnitude of the lake outburst, in terms of the discharge volume, is among the largest reported for glacial lakes in Patagonia and other regions. Glaciar Perito Moreno in the SPI has repeatedly blocked a channel connecting Brazo Rico to Canal de los Témpanos<sup>44–46</sup>. Rupture of the ice dam caused the drainage of lakewater from Brazo Rico to Canal de los Témpanos. During the largest event occurred in 1954–1956 (refs. 43–47), the lake level dropped by 26 m and 5.2 km<sup>3</sup> of water drained<sup>47</sup>. Large GLOFs were reported also in the Northern Patagonia Icefield (NPI)<sup>48–50</sup>. The largest event in the NPI since the 20th century occurred in 2008 at Cachet Lake, a proglacial lake of Glaciar Colonia. The water volume drained during the event was estimated as 0.2 km<sup>3</sup> (ref. 47).

Outbursts of subglacial lakes in Iceland (jökulhlaup) are another example of large-scale glacial lake drainage. Outbursts from Grímsvötn, a subglacial lake beneath Vatnajökull, were estimated to be 4.5 and 0.6–1.2 km<sup>3</sup> for events occurring in the 1930s and 1980s, respectively<sup>51</sup>. An ice-dammed lake formed by advance of Hubbard Glacier, Alaska, released 5.4 km<sup>3</sup> of water when the ice

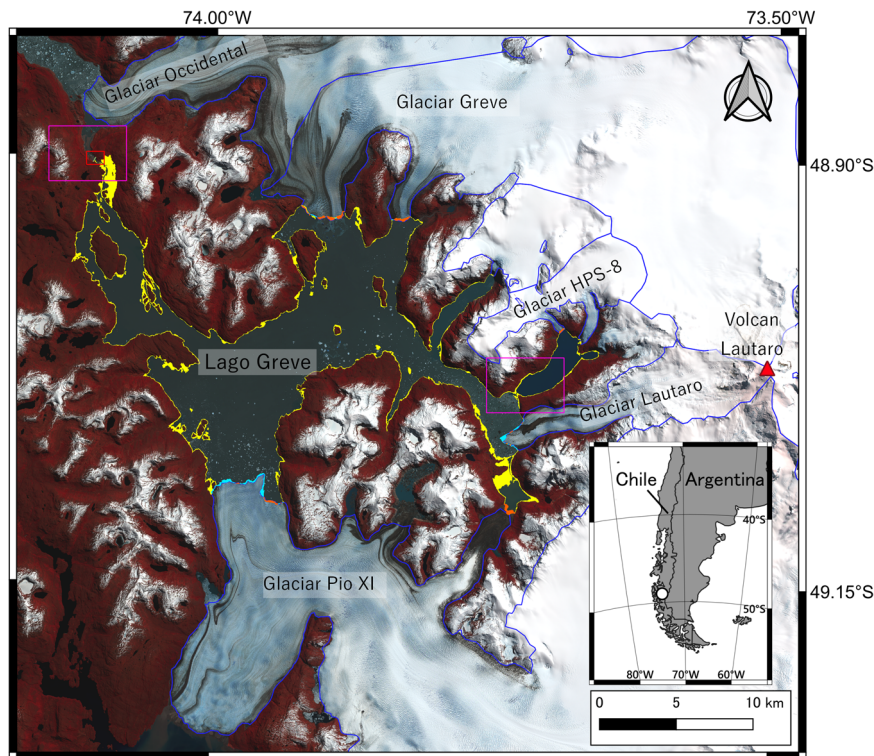


**Fig. 1 Study site.** Satellite image of Lago Greve (Sentinel-2 MSI image on 1st November 2020). The inset shows the location of the study site in South America. The area which turned from lake to land surface from 8 April to 1st November 2020 are highlighted in yellow. Areas highlighted in orange and cyan indicate advance and retreat of glacier calving fronts during the same period. Blue curves indicate glacier boundaries from RGI 6.0 inventory<sup>69</sup> (based on satellite imagery in 2000–2003), with glacier frontal margins delineated in this study. The red box in the upper left corner indicates the location of the lake outlet and the area shown in Fig. 4. The magenta boxes indicate the areas shown in Fig. 3.

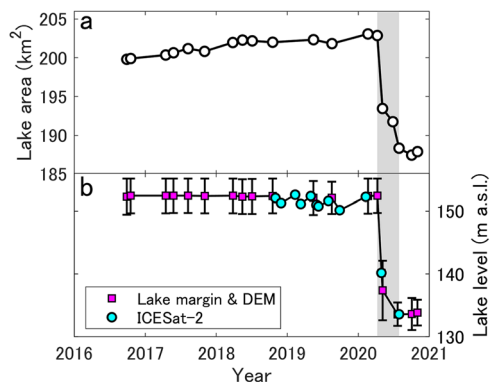


**Fig. 2 Changes in lake area and water level of Lago Greve.** **a** Area and **b** water level of Lago Greve from 28 September 2016 to 1st November 2020. Lake levels indicated by squares were measured by DEMs, while those indicated by circles were obtained by ICESat-2. Gray shaded area indicates the approximate period of the lake drainage event (from 9 April to 29 July 2020). Errorbars represent uncertainty of measurement.

dam collapsed in 1986 (ref. 52). In east Greenland, a glacier-dammed lake Catalina caused four outburst events between 1966 and 2016 (ref. 36). The outbursts were triggered by flotation of the ice dam, which lead to rapid water discharge of 2.6–3.4 Gt. The water volume drained from Lago Greve is comparable to those reported for the previously observed large GLOF events.

**Cause of the drainage.** Satellite images showed that the channel leading lakewater to the lake outlet shifted its flowline after the event. Before the event, in February 2013, the northward water

stream was deflected to west by a ~100 m long bump covered with vegetation at the top of the waterfall (Fig. 4a, c). After the event (21 July 2020), the bump disappeared and the stream shifted northeastward by several hundred meters for a region extending 250 and 300 m up- and down-stream from the outlet, respectively (Fig. 4b, d). Vegetation disappeared from the region bounded by the stream flowlines before and after the event, implying that the northern bank of the stream was eroded over the course of the flowline migration.

Comparison of the DEMs in February 2000 and July 2020 indicates large change in the land surface elevation on the northern bank of the outlet stream (Fig. 4e, f). Elevation dropped by more than 30 m in the region between the lake and the waterfall (highlighted in red in Fig. 4a). Mean elevation change was  $-24.7 \pm 5.6$  m along the flowline of the stream before the event (Z–X' in Fig. 4e) (Fig. 4g) and  $-33.7 \pm 5.6$  m along the flowline after the event (Z'–X' in Fig. 4h). Change in the topography near the waterfall was clearly observed by comparing the cross sections across the flowline (Fig. 4i). Before the event, the stream was running along the depression situated relatively south in the valley (Z in Fig. 4i). Because the surface elevation on the northern bank of the stream dropped by ~20–30 m, the depression shifted to the north by ~100 m and deepened by ~20 m (Z' in Fig. 4i), which is approximately equal to the change in the lake surface elevation after the lake drainage.

Based on these analyses of the satellite images and DEMs, we interpret the mechanism of the outburst as below. Between 9 and 19 April 2020, the bump at the top of the waterfall collapsed (Fig. 4c, d) so that the stream changed its flow direction to north across the bump location. Because of the change in the flow direction, water began eroding the northern bank of the stream. As the erosion proceeded upstream and the valley deepens, the stream gradually

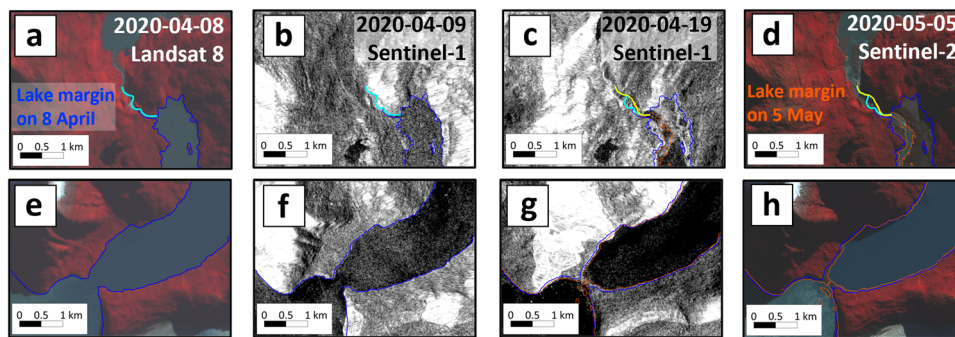


**Fig. 3** Satellite images showing initiation of the drainage event. The images were acquired by Landsat-8, Sentinel-1, Sentinel-2 for the locations indicated by the magenta boxes in Fig. 1a. The acquisition dates are (a and e) 8 April 2020, (b and f) 9 April 2020, (c and g) 19 April 2020, and (d and h) 5 May 2020. Cyan and yellow lines in a–d indicate the outlet stream as observed on the optical images on 8 April and 5 May, respectively. The blue and orange lines are the same for the lake margin.

shifted to the north and the water surface dropped. Most likely, the erosion was accelerated by progressive increase in the discharge from the lake. Elevation change near the bump clearly showed formation of a deep V-shaped valley after the event, suggesting erosion by the stream water (Supplementary Note 1 and Supplementary Fig. 1). We conclude that the collapse of the bump triggered the change in the flow path of the stream, which resulted in the erosion of the valley and the drainage of lakewater.

We speculate that the stream eroded unconsolidated glacial deposits left by the advance of Glacier Occidental during the Little Ice Age (LIA). The front position of the glacier was approximately at the lake outlet in the ~1870s<sup>53,54</sup> (dotted line in Fig. 4a), and the region around the outlet was covered with a moraine formed in front of the glacier<sup>55</sup> (gray line in Fig. 4a). Therefore, it is likely that the region was mantled with glacial deposits as well as sediments carried by lakewater.

The satellite images implied that the event was triggered by the collapse of the bump. However, we do not have information to identify the cause of the collapse. Since flowline of the stream showed no change from April 2000 to 8 April 2020, the process of the collapse was relatively rapid. Given the long distance from the glaciers (>20 km), the impulse of a wave induced by calving is not a likely trigger. Waves due to landslide or rockfall into the lake are not likely as well, because no trace of such an event was found along the lake shore near the outlet. We also exclude an influence of intensive snow/ice melt because the onset of the event was in April. A relatively small earthquake (magnitude 5.2) was recorded on 5 April 2020 at a depth of 13.6 km and a distance of ~200 km from the lake outlet (west of Cochrane, Chile) (USGS, <https://earthquake.usgs.gov/earthquakes/eventpage/us10007exm/origin/detail>, last access: 5 December 2021). Nevertheless, this earthquake was at least four days before the onset of the outburst, and probably too weak to destroy the bump. There is no weather station around the lake, but no extraordinary event was found in the weather conditions in the ERA5 reanalysis dataset<sup>56</sup> (Supplementary Note 2 and Supplementary Fig. 2). A field survey is required to investigate the triggering mechanism details further.

Presumably, the collapse of the bump was not directly related to recent warming climate. However, assuming the bump was composed of morainic materials deposited about 1870, the collapse occurred ~150 years after the retreat of Glacier Occidental. Harrison et al.<sup>32</sup> proposed that GLOF occurs more frequently in the near future as a lagging response to warming climate. The studied event can be regarded as such a delayed response to the changing climate.

**Gravity field.** Total masses of mascon (mass concentration) of land tiles averaged within 200, 300, and 400 km from the lake

showed similar temporal patterns (Fig. 5a). Seasonal variations, clear in the signal as winter positive and summer negative changes, can be attributed to snow accumulation and snow/ice melting. The negative trend over the entire period indicates the mass loss of the glaciers in the region<sup>57,58</sup>. The GRACE data deviate from the fitting curve largely after 2020 (Fig. 5b–d). Root mean square errors (RMSEs) from January 2020 to August 2021 (0.26–0.54 m w.e.) are substantially greater than those for the 2002–2019 period ( $4.6\text{--}7.1 \times 10^{-2}$  m w.e.). The model underestimates the mass loss in this region, implying additional mass loss event there. The RMSEs after July 2020 can be minimized by assuming an additional mass reduction event which took place linearly from April to July 2020 (red curves in Fig. 4b–d). The regression of the data suggested additional mass losses of  $-0.29 \pm 0.03$ ,  $-0.23 \pm 0.02$ , and  $-0.17 \pm 0.02$  m w.e. for the regions within 200, 300, and 400 km, respectively.

Mascon tiles showing negative mass changes from March to August 2020 lie mostly within ~200 km from Lago Greve (Fig. 5e). There the average seasonal changes from March to August in 2002–2019 are already removed from the results. The mass loss regions do not coincide with the Patagonia Icefields (regions within blue curves in Fig. 5e) but are localized near the lake. Therefore, the observed mass loss signals are most likely due to the observed discharge of lakewater from Lago Greve in 2020.

The GRACE data suggested a range of mass loss from  $-0.29$  to  $-0.17$  m w.e. for the regions within 200–400 km, which correspond to the water volume of 33.4–58.5 km<sup>3</sup>. These estimates are substantially greater than the actual volume of the discharge ( $3.7 \pm 0.2$  km<sup>3</sup>) quantified from the change in the lake surface elevation. The discrepancy would be due to the poor spatial resolution of the GRACE gravimetry. Such an intrinsic low resolution reflects the satellite altitudes larger than the lake size by more than an order of magnitude. Lago Greve is the fourth largest glacial lake in the world, but it occupies only 1.5% of a typical CSR mascon tile ( $124 \times 10^2$  km<sup>2</sup>) (ref. <sup>59</sup>). A previous study reported that quantification of water volume changes by GRACE is not suitable even for larger glacial lakes<sup>37</sup>. Thus, we conclude that the satellite gravimetry is able to detect large-scale lake outburst events, but care should be taken for quantification of the water discharge. The importance of GRACE in studying GLOF would be increased if mascon solution is adapted for localized events.

**Implications for calving glaciers.** The sudden drop in the lake level should have impacts on the glaciers terminating in the lake. Previous studies on ice marginal lakes reported impacts of outburst floods on glacier dynamics (e.g., refs. <sup>27,60</sup>). Nevertheless, observation of outburst of a proglacial lake is sparse, thus its impact on the calving front is poorly understood.

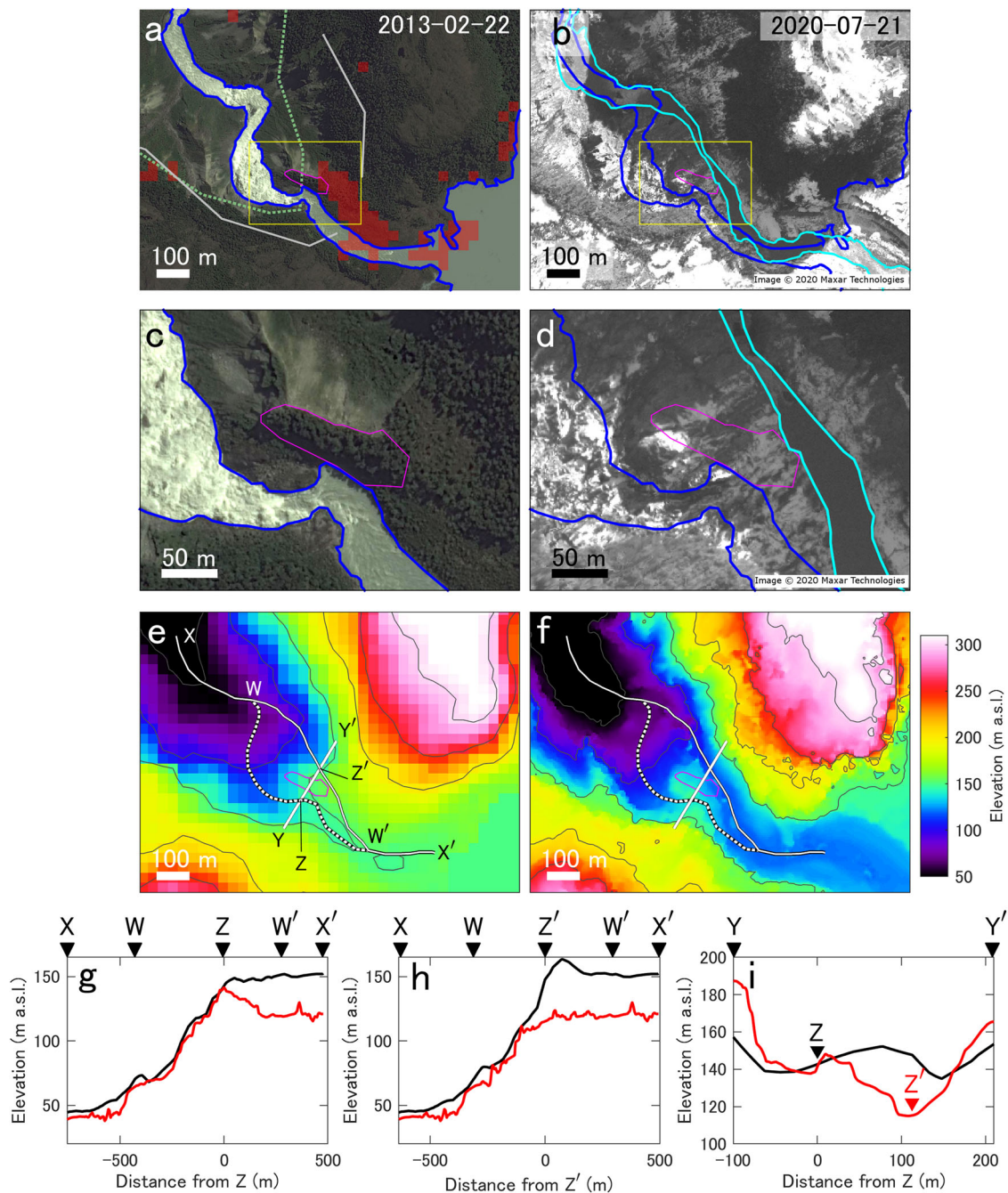


**Fig. 4** Surface elevation changes in the lake outlet region. Satellite images acquired **a** before (Google Earth on February 22, 2013) and **b** after the outburst event (World View-2 ©Maxar on July 21, 2020). Magenta curve in **a** indicates the location of the bump described in the text. Blue and cyan curves in **b** indicate side margins of the outlet stream before and after the event. Green dotted and gray solid lines in **a** indicate the frontal position of Glacier Occidental during the Little Ice Age<sup>52</sup> and its moraine position<sup>54</sup>, respectively. Regions highlighted in red in **a** are where surface elevation decreased by >30 m between 11–22 February 2000 and 21 July 2020. Yellow boxes in **a** and **b** show the regions enlarged in **c** and **d**, respectively. Surface elevation near the outlet of Lago Greve based on **e** SRTM-DEM (February 2000) and **f** WV-DEM (21 July 2020). Dashed and solid curves indicate the flowlines of the stream before and after the event, respectively. **g** Surface elevation along the stream before (X–Z–X' in **e**) and **h** after the event (X–Z'–X'), and **i** across the outlet region (Y–Y').

Considering the tidal influence on the ice speed of marine-terminating glaciers (e.g., ref. <sup>61</sup>), speed change of the glaciers is expected after the outburst of Lago Grave. Further, the drop in the lake level should affect the frequency and magnitude of calving, as well as underwater ice front melting. Therefore, continuing to monitor the glaciers in the future is a unique opportunity to investigate the dynamics and frontal ablation of freshwater calving glaciers.

## Conclusions

In this study, we reported an outburst of Lago Greve in Patagonia, one of the largest glacial lakes in the world. Satellite data showed abrupt lake drainage between 9 and 19 April 2020 and lakewater discharge from April to July 2020. During the event, lake area decreased by  $14.5 \pm 0.02 \text{ km}^2$  and the water level dropped by  $18.3 \pm 1.2 \text{ m}$ . Water volume released from the lake was  $3.7 \pm 0.2 \text{ km}^3$  ( $3.7 \pm 0.2 \text{ Gt}$ ), which indicates the event is among

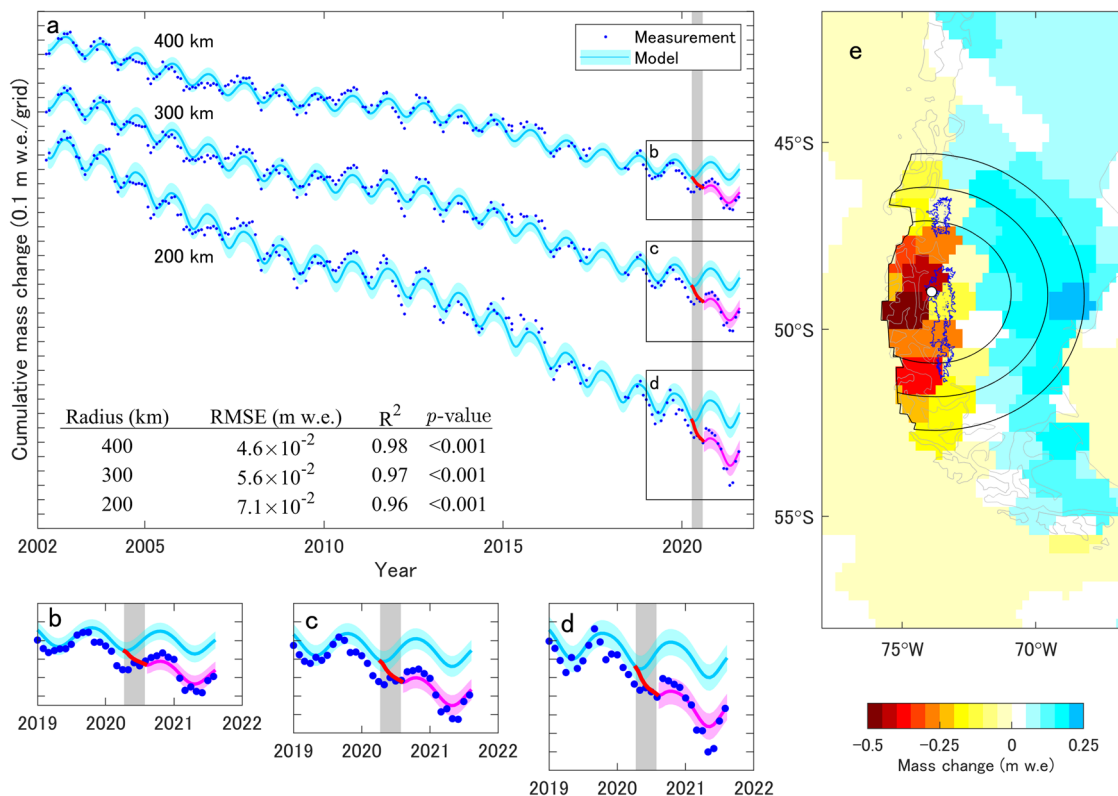


**Fig. 5 Mass changes over the study region.** **a** Mass changes in the GRACE mascon solution summed over areas within 200, 300, and 400 km from the lake. Cyan curves are the best-fit time series assuming Eq. 2. RMSEs of the model are shown by the shading around the curves. Red and magenta curves are results of the regression assuming an additional mass loss event that occurred at a constant rate from 8 April to 29 July 2020 (gray shaded band). RMSEs, correlation coefficients,  $p$ -values of the fitting are also shown. **b-d** shows the close-up view of the parts after 2019. **e** Distribution of mass changes from March to August, 2020. Regions within blue curves indicate the Patagonia Icefields. The white dot indicates the location of Lago Greve. Solid curves indicate the regions within 200, 300, 400 km from the lake.

the largest GLOFs ever reported. The outburst was triggered by the collapse of a bump near the lake outlet and subsequent change in the flow path of the outlet stream. This event activated the erosion of the bank and the bed of the stream, resulting in lakewater drainage through a deepened valley. The event was also detected by the gravity field observed by the GRACE/GRACE-FO mascon solution. The GRACE data largely overestimate the volume of water release because its spatial resolution is not sufficient for the GLOF event. Thus, care should be taken when mascon solution is used to quantify the magnitude of a lake outburst.

## Methods

**Lake area.** The area of Lago Greve was measured from 28 September 2016 to 1st November 2020, using 19 satellite images acquired by the Sentinel-2 Multispectral Imager (MSI) and Landsat 8 Operational Land Imager (OLI). The spatial resolution of the images were 10 m and 30 m, respectively (Supplementary Table 1). The lake margin was manually delineated on false-color composite images on the QGIS geographic information system software. False-color images were converted from near-infrared, green and red band images (bands 8, 4, 3 of Sentinel-2 MSI, and 5, 4, 3 of Landsat 8 OLI). We utilized normalized differential water index (NDWI) to distinguish water and land in regions covered by shades (Supplementary Note 3 and Supplementary Fig. 3). NDWI is commonly used to detect water bodies in satellite images. The index is defined as

$$\text{NDWI} = \frac{R_G - R_{\text{NIR}}}{R_G + R_{\text{NIR}}} \quad (1)$$

where  $R_G$  and  $R_{\text{NIR}}$  are the reflectance of green and near-infrared bands at the top of the atmosphere (e.g., ref. 62). To evaluate the contributions of glacier retreat and advance to the lake area, changes in the glacier areas near the front were also measured by the images. To constrain the onset of the drainage event, we also used backscatter images of synthetic aperture radar (SAR) obtained by Sentinel-1 satellites (Fig. 3b, c, f, g).

Uncertainty in the lake area was estimated by assuming that the individual measurement along the lake margin has an error up to the image resolution. Lake area computation was repeated 1000 times by randomly shifting the nodes of the lake polygon within the range of the resolution. Standard deviation of the repeated computation was  $\pm 0.02 \text{ km}^2$  for both of the MSI and OLI images. The uncertainty in the glacier area change was separately evaluated based on the uncertainty in the ice-front positions reported for the same procedure<sup>63</sup> ( $\pm 7 \text{ m}$ ).

**Lake water level.** Water surface elevation of Lago Greve was measured from 28 September 2016 to 1st November 2020 with intervals of five days to six months, based on satellite laser altimetry and DEMs.

Data from the Advanced Topographic Laser Altimeter System (ATLAS) mounted on Ice, Cloud, and Land Elevation Satellite-2 (ICESat-2) was analyzed during a period from November 2018 to July 2020 (Supplementary Table 2). In this study, we used ICESat-2/ATLAS L3A Inland Water Surface Height products (ATL13), which provide lake- and river-surface heights above the Earth Gravitational Model 2008 mean sea level<sup>64</sup>. We used the ATL13 point data obtained within the lake area. Data acquired on the same day were averaged and the standard deviations were taken as a measure of uncertainty.

From September 2016 to November 2020, the lake level was also measured by reading elevation along the lake margin from DEMs. We used a DEM derived from the Shuttle Radar Topography Mission (SRTM-DEM) on February 2000, which is distributed by the U.S. Geological Survey (USGS). Spatial resolution and uncertainty in the vertical coordinates of the SRTM-DEM were 30 and  $\pm 7 \text{ m}$ , respectively<sup>65</sup>. To obtain the elevation of the lake shore which emerged after the onset of the drainage (April–November 2020), we generated a 5-m resolution DEM by applying a photogrammetric technique to a stereo pair World View-2 satellite images acquired on 21 July 2020 (WV-DEM, Supplementary Note 4). The accuracy of the DEM was estimated as  $\pm 5.6 \text{ m}$  (Supplementary Note 4 and Supplementary Fig. 4). Vertical offsets of the DEMs against the altimetry data were corrected by comparing lake-surface elevation from the DEMs with those obtained by altimetry within seven days. The mean difference from the altimetry data ( $+2.5 \text{ m}$  for SRTM-DEM and  $-1.4 \text{ m}$  for WV-DEM) was used for the correction of the DEM derived lake level. Data during the drainage period was excluded from the offset evaluation because the water level change in seven days was too large.

The SRTM-DEM was used for the period before the drainage event (from September 2016 to April 2020), whereas the WV-DEM was used after the event (from April to November 2020). The DEMs were used also for investigation of the terrain near the outlet of the lake.

To specify the onset of the lake drainage, we inspected backscatter images of Sentinel-1 acquired on 9 and 19 April 2020 (downloaded from the EO browser <https://apps.sentinel-hub.com/eo-browser/>). Spatial resolution of the images was 4.4 m. The SAR images were compared with optical images on 8 April and 5 May 2020 to find changes in the lake margin and outlet stream (Fig. 3).

**GRACE mascon solution.** Monthly mascon data were analyzed in the study region, using mascon solutions distributed by the Center for Space Research (CSR), the University of Texas at Austin<sup>59</sup>. These mascon solutions were derived by GRACE and GRACE-FO satellite gravimetry systems. Geodesic grids were located on the earth surface with intervals of ~120 km. Note that the CSR mascon product is provided as a 0.5° grid data set, which was generated by resampling original mascon solution. Changes in the mass from April 2002 to December 2019 were averaged over regions within 200, 300, 400 km from the center of the lake (Fig. 4c) considering the resolution of the GRACE measurement of 200–400 km (ref. 66). We modeled the mascon time-series with a function composed of linear, seasonal, and decadal variation terms.

$$M(t) = \sum_{i=1}^3 \left( k_{2i-1} \sin \frac{2\pi}{T_i} t + k_{2i} \cos \frac{2\pi}{T_i} t \right) + k_7 t + k_8 \quad (2)$$

$M$  is the time-variable mass,  $t$  is the elapsed time since 16 April 2002,  $T_{i=1-3}$  indicate periods of annual, semiannual and decadal cycles, and  $k_{1-8}$  are coefficients estimated by the least-squares method. We also compared the spatial distribution of mascon in March and August 2020. To eliminate seasonal variations, the data sets were corrected for mean differences between March and August observed from 2002–2019.

## Data availability

Timeseries of lake margin, lake area, water level, mascon solutions are deposited and available at Zenodo repository<sup>67</sup> (<https://doi.org/10.5281/zenodo.5781833>).

## Code availability

Map figure of the Study site (Fig. 1) was generated by using an open-source GIS software (QGIS 3.22). Other figures were generated by using MATLAB 2018b (<https://mathworks.com/products/matlab.html>). The MATLAB scripts were written with standard MATLAB functions and functions included a freely available toolbox as M\_Map version 1.4 m (ref. 68).

Received: 5 January 2022; Accepted: 11 August 2022;

Published online: 26 August 2022

## References

- Shugar, D. H. et al. Rapid worldwide growth of glacial lakes since 1990. *Nat. Climate Change*. **10**, 939–945 (2020).
- Wilson, R. et al. Glacial lakes of the Central and Patagonian Andes. *Global Planetary Change*. **162**, 275–291 (2018).
- Field, H. R., Armstrong, W. H. & Huss, M. Gulf of Alaska ice-marginal lake area change over the Landsat record and potential physical controls. *The Cryosphere*. **15**, 3255–3278 (2021).
- Zhang, G., Yao, T., Xie, H., Wang, W. & Yang, W. An inventory of glacial lakes in the Third Pole region and their changes in response to global warming. *Global Planetary Change*. **131**, 148–157 (2015).
- Mallalieu, J., Carrivick, J. L., Quincey, D. J. & Raby, C. L. Ice-marginal lakes associated with enhanced recession of the Greenland Ice Sheet. *Global Planetary Change*. **202**, 103503 (2021).
- Truffer, M. & Motyka, R. J. Where glaciers meet water: Subaqueous melt and its relevance to glaciers in various settings. *Rev. Geophys.* **54**, 220–239 (2016).
- Tsutaki, S. et al. Contrasting thinning patterns between lake- and land-terminating glaciers in the Bhutanese Himalaya. *The Cryosphere*. **13**, 2733–2750 (2019).
- Sugiyama, S., Minowa, M., & Schaefer, M. Underwater ice terrace observed at the front of Glacier Grey, a freshwater calving glacier in Patagonia. *Geophys. Res. Lett.* **46**, <https://doi.org/10.1029/2018GL081441> (2019).
- Carrivick, J. L., Tweed, F. S., Sutherland, J. L. & Mallalieu, J. Toward numerical modeling of interactions between ice-marginal proglacial lakes and glaciers. *Front. Earth Sci.* **8**, 577068 (2020).
- King, O., Bhattacharya, A., Bhambri & Bolch, T. Glacial lakes exacerbate Himalayan glacier mass loss. *Sci. Reports*. **9**, 18145 (2019).
- Minowa, M., Schaefer, M., Sugiyama, S., Sakakibara, D. & Skvarca, P. Frontal ablation and mass loss of the Patagonian icefields. *Earth Planetary Sci. Lett.* **561**, 116811 (2021).
- Abdel Jaber, W., Rott, H., Floricioiu, D., Wuite, J. & Miranda, N. Heterogeneous spatial and temporal pattern of surface elevation change and mass balance of the Patagonian ice fields between 2000 and 2016. *The Cryosphere*. **13**, 2511–2535 (2019).
- Dussaillat, L., Berthier, E. & Brun, F. Geodetic Mass Balance of the Northern Patagonian Icefield from 2000 to 2012 Using Two Independent Methods. *Front. Earth Sci.* **6**, 8 (2018).
- Sakakibara, D. & Sugiyama, S. Ice-front variations and speed changes of calving glaciers in the Southern Patagonia Icefield from 1984 to 2011. *J. Geophys. Res.: Earth Surf.* **119**, 2541–2554 (2014).
- Zemp, M. et al. Global glacier mass changes and their contributions to sea-level rise from 1961 to 2016. *Nature* **568**, 382–386 (2019).
- Sommaruga, R. When glaciers and ice sheets melt: consequences for planktonic organisms. *J. Plankton Res.* **37**, 509–518 (2015).
- Tiberti, R. et al. Food Web Complexity of High Mountain Lakes is Largely Affected by Glacial Retreat. *Ecosystems* **23**, 1093–1106 (2020).
- Sugiyama, S. et al. Thermal structure of proglacial lakes in Patagonia. *J. Geophys. Res.: Earth Surf.* **121**, 2270–2286 (2016).
- Sugiyama, S. et al. Subglacial discharge controls seasonal variations in the thermal structure of a glacial lake in Patagonia. *Nat. Commun.* **12**, 6301 (2021).
- Carrivick, J. L. & Tweed, F. S. Proglacial lakes: character, behaviour and geological importance. *Quaternary Sci. Rev.* **78**, 34–52 (2013).
- Meerhoff, E., Castro, L. R., Tapia, F. J. & Pérez-Santos, I. Hydrographic and Biological Impacts of a Glacial Lake Outburst Flood (GLOF) in a Patagonian Fjord. *Estuaries Coasts*. **42**, 132–143 (2019).
- Glasser, N. F. et al. Glacial lake drainage in Patagonia (13–8 kyr) and response of the adjuacent Pacific Ocean. *Sci. Reports*. **6**, 21064 (2016).
- Thorndyraft, V. R. et al. Glacial lake evolution and Atlantic-Pacific drainage reversals during deglaciation of the Patagonian Ice Sheet. *Quaternary Sci. Rev.* **203**, 102–127 (2019).
- Neupene, R., Chen, H. & Cao, C. Review of moraine dam failure mechanism. *Geo. Natural Hazards Risk* **10**, 1948–1966 (2019).
- Hubbard, B. et al. M.J. Impact of a rock avalanche on a moraine-dammed proglacial lake: Laguna Safuna Alta, Cordillera Blanca, Peru. *Earth Surf. Processes Landforms*. **30**, 1251–1264 (2005).
- Westby, M. J. et al. Modelling outburst floods from moraine-dammed glacial lakes. *Earth-Sci. Rev.* **134**, 137–159 (2014).
- Sugiyama, S., Bauder, A., Huss, M., Riesen, P. & Funk, M. Triggering and drainage mechanisms of the 2004 glacier-dammed lake outburst in Gornergletscher, Switzerland. *J. Geophys. Res.* **113**, F04019 (2008).
- Emmer, A. & Cochachin, A. The causes and mechanisms of moraine-dammed lake failures in the Cordillera Blanca, North American Cordillera, and Himalayas. *AUC Geographica*. **48**, 5–13 (2013).
- Veh, G., Korup, O. & Walz, A. Hazard from Himalayan glacier lake outburst floods. *Proc. Nat. Academy Sci.* **117**, 907–912 (2020).
- Carrivick, J. L. & Tweed, F. S. A global assessment of the societal impacts of glacier outburst floods. *Global Planetary Change*. **144**, 1–16 (2016).
- Emmer, A. et al. 160 glacial lake outburst floods (GLOFs) across the Tropical Andes since the Little Ice Age. *Global Planetary Change* **208**, 103722 (2022).
- Harrison, S. et al. Climate change and the global pattern of moraine-dammed-glacial lake outburst floods. *The Cryosphere*. **12**, 1195–1209 (2018).
- Nie, Y. et al. A regional-scale assessment of Himalayan glacial lake changes using satellite observations from 1990 to 2015. *Remote Sensing Environ.* **189**, 1–13 (2017).
- Xu, N. et al. Global Estimation and Assessment of Monthly Lake/Reservoir Water Level Changes Using ICESat-2 ATL13 Products. *Remote Sensing*. **13**, 2744 (2021).
- Jiang, L., Nielsen, K., Andersen, O. B. & Bauer-Gottwein, P. Monitoring recent lake level variations on the Tibetan Plateau using CryoSat-2 SARIn mode data. *J. Hydrology*. **544**, 109–124 (2017).
- Grinsted, A., Hvidberg, C. S., Campos, N. & Dahl-Jensen, D. Periodic outburst floods from an ice-dammed lake in East Greenland. *Sci. Reports*. **7**, 9966 (2017).
- Carabajal, C. C. & Boy, J.-P. Lake and reservoir volume variations in South America from radar altimetry, ICESat laser altimetry, and GRACE time-variable gravity. *Adv. Space Res.* **68**, 652–271 (2021).
- Pereira, A., Cornero, C., Matos, A. C. O. C., Pacino, M. C. & Blitzkow, D. Detection of total water mass changes in the Patagonian glaciers area by satellite gravimetry. *Geofísica Int.* **60**, 161–174 (2021).
- Yi, S. et al. The potential of GRACE gravimetry to detect the heavy rainfall-induced impoundment of a small reservoir in the upper Yellow River. *Water Resource Res.* **53**, <https://doi.org/10.1002/2017WR020793> (2017).

40. Warren, C. R. & Rivera, A. Non-linear climatic response of calving glaciers: a case study of Pio XI Glacier, Chilean Patagonia. *Revista Chilena de Historia Nat.* **67**, 385–394 (1994).
41. Warren, C. R., Rivera, A. & Post, A. Greatest holocene advance of Glacier Pio XI, Chilean Patagonia: possible causes. *Annals Glaciology* **24**, 11–15 (1997).
42. Rivera, A. El Glacier Pio, XI: Avances y retrocesos, El impacto sobre su entorno durante el presente siglo. *Revista Geografica de Chile Terra Australis*. **36**, 33–62 (1992).
43. Malz, P. et al. Elevation and mass changes of the Southern Patagonia Icefield derived from TanDEM-X and SRTM data. *Remote Sensing*. **10**, 1–17 (2018).
44. Stuefer, M., Rott, H. & Skvarca, P. Glacier Perito Moreno, Patagonia: Climate sensitivities and glacier characteristics preceding the 2003/04 and 2005/06 damming events. *J. Glaciology* **53**, 3–16 (2007).
45. Lenzano, M. G. et al. Analyzing the oscillations of the Perito Moreno Glacier, using time-lapse image sequences. *Cold Regions Sci. Technol.* **146**, 155–166 (2018).
46. Pasquini, A. I. & Deptris, P. J. Southern Patagonia's Perito Moreno Glacier, Lake Argentino, and Santa Cruz River hydrological system: An overview. *J. Hydrology*. **405**, 48–56 (2011).
47. Heinsheimer, G. J. Zur Hydrologie und Glaziologie del Lago Argentino und Ventisquero Moreno III. *Zeitschrift für Gletscherkunde and Glazialgeologie* **4**, 61–72 (1958).
48. Dussaillant, A. et al. Repeated glacial-lake outburst floods in Patagonia: an increasing hazard? *Natural Hazards* **54**, 469–481 (2010).
49. Aniya, M. et al. GLOFs of Laguna de los Témpanos, glacier-dammed side lake of Glacier Steffen, Hielo Patagónico Norte, Chile, since 1974. *Bulletin Glaciological Res.* **38**, 13–24 (2020).
50. Wilson, R. et al. The 2015 Chileno Valley glacial lake outburst flood, Patagonia. *Geomorphology* **332**, 51–65 (2019).
51. Gudmundsson, M. T., Björnsson, H. & Pálsson, F. Changes in jökulhlaup sizes in Grímsvotn, Vatnajökull, Iceland, 1934–91, deduced from in-situ measurements of subglacial lake volume. *J. Glaciological* **41**, 263–272 (1995).
52. Mayo, L. R. Advance of Hubbard Glacier and 1986 outburst of Russell Field, Alaska, U.S.A. *Annals Glaciological*. **13**, 189–194 (1989).
53. Meier, W. J.-H., Griefinger, J., Hochreuther, P. & Braun, M. H. An Updated Multi-Temporal Glacier Inventory for the Patagonian Andes With Changes Between the Little Ice Age and 2016. *Front. Sci.* **6**, 62 (2018).
54. Davies, B. & Glasser, N. Accelerating shrinkage of Patagonian glaciers from the little ice age (~AD 1870) to 2011. *J. Glaciological*. **58**, 1063–1084 (2012).
55. Davies, B. J. et al. The evolution of the Patagonian Ice Sheet from 35 ka to the present day (PATICE). *Earth-Sci. Rev.* **204**, 103152 (2020).
56. Hersbach, H., & Dee, D. ERA reanalysis is in production. Available at: <https://www.ecmwf.int/en/newsletter/147/news/era5-reanalysis-production> (2016).
57. Chen, J. L., Wilson, C. R., Tapley, B. D., Blankenship, D. D. & Ivins, E. R. Patagonia Icefield melting observed by Gravity Recovery and Climate Experiment (GRACE). *Geophys. Res. Lett.* **34**, L22501 (2007).
58. Li, J., Chen, J., Ni, S., Tang, L. & Hu, X. Long-term and inter-annual mass changes of Patagonia Ice Field from GRACE. *Geodesy and Geodynamics*. **10**, 100–109 (2019).
59. Save, H., Bettadpur, S. & Tapley, B. D. High resolution CSR GRACE RL05 mascons. *J. Geophys. Res.: Solid Earth*. **121**, 7547–7569 (2016).
60. Bigelow, D. G. et al. The role of englacial hydrology in the filling and drainage of an ice-dammed lake, Kaskawulsh Glacier, Yukon, Canada. *J. Geophys. Res.: Earth Surf.* **125**, e2019JF005110 (2020).
61. Podolskiy, E. A. et al. Tide-modulated ice flow variations drive seismicity near the calving front of Bowdoin Glacier, Greenland. *Geophys. Res. Lett.* **43**, 2036–2044 (2016).
62. McFeeters, S. K. Using the normalized difference water Index (NDWI) within a geographic information system to detect swimming pools for mosquito abatement: a practical approach. *Remote Sensing*. **5**, 3544–3561 (2013).
63. Hata, S. & Sugiyama, S. Changes in the Ice-Front Position and Surface Elevation of Glacier Pío XI, an Advancing Calving Glacier in the Southern Patagonia Icefield, From 2000–2018. *Front. Earth Sci.* **8**, 576044 (2021).
64. Jasinski, M. F. et al. ATLAS/ICESat-2 L3A Inland Water Surface Height, Version 2 [Data Set]. Boulder, Colorado USA. *NASA National Snow and Ice Data Center Distributed Active Archive Center*. <https://doi.org/10.5067/ATLAS/ATL13.002> (2019).
65. Rignot, E., Rivera, A. & Casassa, G. Contribution of the Patagonia icefields of South America to sea level rise. *Science* **302**, 434–437 (2003).
66. Sasgen, I., Konrad, H., Helm, V. & Grosfeld, K. High-Resolution Mass Trends of the Antarctic Ice Sheet through a Spectral Combination of Satellite Gravimetry and Radar Altimetry Observations. *Remote Sensing*. **11**, 144 (2019).
67. Hata, S., Sugiyama, S. & Heki, K. Timeseries of lake margin, lake area, water level, mascon solutions of Lago Greve [Data set], *Zenodo*, <https://doi.org/10.5281/zenodo.5781833>.
68. Pawlowicz, R. "M\_Map: A mapping package for MATLAB", version 1.4m, [Computer software], available online at [www.eoas.ubc.ca/~rich/map.html](http://www.eoas.ubc.ca/~rich/map.html) (2020).
69. RGI Consortium. Randolph glacier inventory – a dataset of global glacier outlines: version 6.0: technical report. Available at: <https://doi.org/10.7262/N5-RGI-60> (2017).

## Acknowledgements

The authors thank Chiyuki Narama and Masahiro Minowa for helpful discussions. Dan Shugar kindly provided the detail of a glacial lake inventory and Evgeny A. Podolskiy helped us with seismic data in the study region. We thank three anonymous reviewers for constructive comments on the manuscript. This research was funded by JSPS KAKENHI grant 20H00186 (2020–2025) and JST SPRING, Grant Number JPMJSP2119 (2021–2022). K.H. is supported by Chinese Academy of Sciences, President's International Fellowship Initiative (Grant number 2022VEA0014). The English was corrected by Ariah Kidder. Landsat images and SRTM DEM were downloaded from <http://earthexplorer.usgs.gov/>. Sentinel images were downloaded from <https://scihub.copernicus.eu/dhus/>. GRACE/GRACE-FO CSR RL06 Mascon solution was downloaded from [http://www2.csr.utexas.edu/grace/RL06\\_mascons.html](http://www2.csr.utexas.edu/grace/RL06_mascons.html). ERA5 reanalysis data was downloaded from <https://cds.climate.copernicus.eu/>.

## Author contributions

S.H. processed the data for measurement of lake area, lake water level, and produced the figures. S.H. and S.S. wrote the text. S.H. and K.H. analyzed the GRACE data. All authors contributed to discussion and manuscript preparation.

## Competing interests

Shin Sugiyama is an Editorial Board Member for Communications Earth & Environment, but was not involved in the editorial review of, nor the decision to publish this article. All other authors declare no competing interests.

## Additional information

**Supplementary information** The online version contains supplementary material available at <https://doi.org/10.1038/s43247-022-00531-5>.

**Correspondence** and requests for materials should be addressed to Shuntaro Hata.

**Peer review information** *Communications Earth & Environment* thanks Silvana Moragues and the other, anonymous, reviewer(s) for their contribution to the peer review of this work. Primary Handling Editors: Joe Aslin. Peer reviewer reports are available.

**Reprints and permission information** is available at <http://www.nature.com/reprints>

**Publisher's note** Springer Nature remains neutral with regard to jurisdictional claims in published maps and institutional affiliations.



**Open Access** This article is licensed under a Creative Commons Attribution 4.0 International License, which permits use, sharing, adaptation, distribution and reproduction in any medium or format, as long as you give appropriate credit to the original author(s) and the source, provide a link to the Creative Commons license, and indicate if changes were made. The images or other third party material in this article are included in the article's Creative Commons license, unless indicated otherwise in a credit line to the material. If material is not included in the article's Creative Commons license and your intended use is not permitted by statutory regulation or exceeds the permitted use, you will need to obtain permission directly from the copyright holder. To view a copy of this license, visit <http://creativecommons.org/licenses/by/4.0/>.

© The Author(s) 2022